MALATYA TURGUT OZAL UNIVERSITY JOURNAL of ENGINEERING and NATURAL SCIENCES Volume 6, Issue 1 (2025) 34-41

NATURENGS
E-ISSN 2717-8013
https://dergipark.org.tr/en/pub/naturengs

Behavior Determination of Rigid Vegetation Effect on Flow Dynamics in Open Channels Using CFD Technology

Mahmut Aydoğdu *

Malatya Turgut Özal University, Department of Civil Engineering, Malatya Türkiye – 44900

ARTICLE INFO

Received 24.04.2025
Accepted 21.06.2025

Doi: 10.46572/naturengs.1682946

ABSTRACT

In recent years, computational fluid dynamics software has significantly contributed to the literature on flow characteristics and turbulent solutions in open channel flows. In this study, two vegetation patch arrangements underwent numerical simulation using the Reynolds Stress Model in Ansys-Fluent software. The flow dynamics of the two cases were compared, and the responses of vegetation patches under subcritical flow conditions were investigated. First, the model was validated and then utilized for numerical simulation. It was observed that more effective velocity reduction occurred in the vegetation patch region and immediately downstream of the patches. While the vegetation patch in Case-1 reduced the flow velocity by 57% compared to the flow velocity at the channel entrance, it remained at 52% for Case-2. The depth-averaged vertical velocity distribution at points P1 and P2 showed lower values downstream for Case-2. Regarding the effect in the downstream region, the turbulence area in Case-2 was narrower compared to Case-1, with turbulent kinetic energy values greater than 0 observed in the channel center. While the energy dissipation percentage was 30% for Case-1, approximately 43% was achieved in Case-2. These results strongly support the feasibility reports with visuals and big data opportunities of CFD sampling before field applications.

Keywords: CFD, rigid vegetation patch, turbulent kinetic energy, open-channel, energy dissipation

1. Introduction

Accurate estimation of flow cross-section in open channel flows is very important for good hydraulic design and flood planning. The main factors determining the flow rate in natural or artificial channels are hydraulic gradient, channel geometry, and flow bed conditions. Dynamic conditions of flow are affected not only by non-living elements such as flow and sediment but also sometimes by living elements such as plants. For this reason, vegetation growing spontaneously in streams and river channels is a remarkable and frequently encountered situation. Because the presence of vegetation is effective both in determining the flow capacity of the channel and on the bottom surface roughness. Here, factors such as plant type, plant diameter, height, shape, flexibility, spatial distribution, and density are the parameters that can affect the flow resistance. Therefore, the vegetation formed causes changes in the hydrodynamic conditions of the flow and thus, sediment transport, nutrient supply, pollutants, dissolved oxygen, and aquatic life are also affected [1,2]. Therefore, vegetation in water helps regulate water levels, improve water quality, reduce flood and inundation damage, provide important fish and wildlife habitats, and support recreational activities. This resistance mechanism, which is especially important in terms of flood safety, needs to be carefully examined. Because in flood control projects, the effects of any obstacles that disturb the flow on the flow rate and flow structure should be well analyzed [3]. The effect of vegetation on flow dynamics has inspired many literature studies. Bai et al. [4] developed a numerical model using the lattice Boltzmann method to examine the hydrodynamic and pollutant transport characteristics in compound cross-section channels. They revealed the significant effect of flexible vegetation on flow patterns. In addition, researchers have emphasized the importance of calculating the hydraulic and hydrodynamic properties of vegetated channel flow in the analysis of floods, which are one of the most important natural disasters caused by climate change,

* Corresponding author. e-mail address: mahmut.aydogdu@ozal.edu.tr
ORCID : 0000-0002-7339-2442

especially when the vegetation in the floodplains, even trees, become part of the flow section due to the overflow of the river bed into the floodplain [5-7].

Considering the importance of the subject, in the last few decades, due to the development of software technologies, studies focused on this subject in the numerical environment have emerged. In particular, significant research has been conducted to understand the chaotic hydrodynamic processes in open channel flow surrounded by vegetation. The effect of different vegetation on the hydrodynamic properties of open channel flow at different levels has been investigated numerically or analytically in many studies [8-12]. Wang et al. [13] focused on the interaction between vegetation, water velocity and sediment transport. They stated that the density and configuration of vegetation have an effect on water velocity at various levels and that the resistance to flow increases as the vegetation density increases. Sabokrouhiyeh et al. [14] used a 2-dimensional numerical model to evaluate the effect of vegetation density on the hydraulic efficiency of wetlands. Yılmazer et al. [15] used the experimental data from the previous study of Yılmazer et al. [16]. For this purpose, they remodeled the same experimental system with FLOW-3D to investigate the effects of fully submerged plants in the open channel on channel flow velocities. They compared the experimental results with this model. Cui and Neary [17] used large eddy simulation (LES) to study turbulent flows with fully submerged vegetation, investigating how organized patterns facilitate momentum movement at the interface between water and vegetation.

Using only the experimental approach, it is difficult to obtain comprehensive details of the flow structure through the vegetation arrangements. Experimental approaches often face difficulties in capturing the complex interactions between flow and vegetation due to the scale, apparatus, and difficulty in accurately measuring the flow dynamics in the vegetated areas [18]. These limitations may lead to an incomplete understanding of the flow structure and its variability under different vegetation arrangements. For this, numerical simulation is the best way to capture the complex flow around these vegetation arrangements. The main objective of the present research is not only to investigate the vegetation patch configurations but also to discuss the flow diversion around these vegetation patches in the natural river. Therefore, numerical simulations were conducted to explore the flow patterns around vegetation patches consisting of large-diameter rigid vegetation pieces with diamond-shaped arrangements. A CFD approach was applied to visualize the detailed flow structures, velocity distribution, depth-averaged velocity distribution, and turbulent kinetic energy around the vegetation patches in single-row and double-row arrangements.

2. Materials and Methods

2.1. Numerical frame setup

It is very important in CFD studies to choose the channel geometry at a level that will provide an economical calculation time. Within the scope of this study, an attempt was made to draw a suitable channel geometry that will obtain three-dimensional solutions. For this purpose, a rectangular channel of 2.75 m length, 0.4 m width, and 0.3 m height was drawn. Inside the open channel, rigid vegetations with a square geometry of 3x3 cm on each side were used and arranged in a diamond shape on the channel center axis, 1 m from the upstream to the downstream side. Previously, Chen et al. [28] conducted analyses using a flexible vegetation structure of equal diameter. A detailed drawing is given in Figure 1. The channel dimensions given in the plan view and the dimensions of the vegetation patch were drawn in cm.

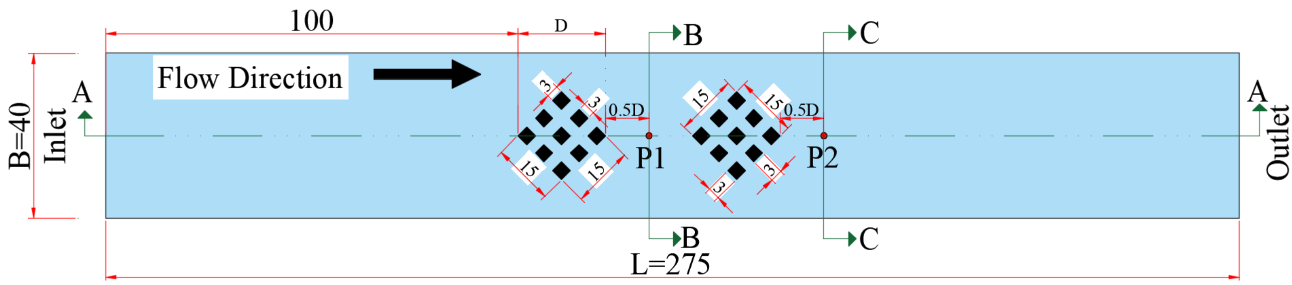

Figure 1. Details of the open channel and vegetation patch.

In Fig. 1, the alignment of two vegetation patches and the measurement points are also given as P1 and P2. For vertical direction measurements of the flow structure, P points were selected 0.5D downstream from the patch. The measurement location was selected according to their importance as reported in previous studies [18,19]. In addition, vertical section A-A and cross sections B-B and C-C were selected to record the detailed velocity and turbulent flow structure along the channel. Here, only vertical measurements at point P1 were performed for a single-row vegetation patch, and measurements considering the velocity and turbulent flow structure were performed at sections A-A and B-B. In addition, other parameters of the flow hydraulics are given in Table 1. Here, Case-1 represents a single-row vegetation patch, while Case-2 represents the channel case with double-row vegetation patches.

Table 1. Parameters considered for numerical solutions Case-1 and Case-2.

Case no	Flow rate ($l.s^{-1}$)	Flow depth (cm)	Inlet velocity ($m.s^{-1}$)	Fr	Re
Case-1	17.85	12.33	0.362	0.33	44635
Case-2	17.85	12.33	0.362	0.33	44635

In numerical solutions, equal input conditions were considered for both Case-1 and Case-2. Here, as seen in Table 1, solutions were carried out under subcritical flow conditions.

2.2. Boundary condition and mesh detail

In this part of the study, the 3D channel area was drawn via the Solidworks program, saved as a (step) extension, and transferred to the Ansys-Fluent software. The channel bottom, side surfaces, and vegetation patches were defined “wall” based on the no-slip wall condition. This condition is widely used in fluid dynamics studies. In particular, it shows that viscous fluids exhibit zero velocity near a solid wall, as shown by Dissanayaka and Tanaka [20] and Asif et al. [5]. Additionally, in this study, the inlet is defined as "velocity inlet", the outlet boundary and the channel ceiling, namely the atmosphere, are defined as "pressure outlet". Here, while the equal inlet velocity is taken as 0.362 $m.s^{-1}$ for both cases, the flow rate value is considered as 17.85 $l.s^{-1}$. Numerical calculations were performed in the Fluent environment using the Reynolds Stress Model (RSM) within the framework of the Reynolds Averaged Navier-Stokes (RANS) method. Eddy-viscosity-based models, including the k-ε and k-ω models, present significant limitations when applied to complex, real-world turbulent flows frequently encountered in engineering contexts. In situations characterized by high anisotropy, pronounced streamline curvature, flow separation, recirculation zones, or flows influenced by mean rotational effects, these models often yield inadequate performance [27]. That's why the primary evidence of RSM's superiority is its ability to capture turbulence anisotropy, especially in regions close to rigid boundaries (walls/floors). Models such as k-ε, which are based on the concept of eddy viscosity, assume that Reynolds stress aligns with the velocity gradient, leading them to consider turbulence isotropic (the same in all directions). However, in real flows, turbulence is not isotropic, particularly near boundaries; turbulence fluctuations perpendicular to the boundary are suppressed, while those parallel to the boundary may increase. RSM was selected for this study due to its ability to accurately capture the complex and anisotropic nature of turbulence around vegetation patches. Unlike simpler models such as Standard k-ε or k-ω that assume isotropic turbulence, RSM provides a more reliable estimate of the turbulent intensity (TI) and momentum change by resolving the Reynolds stresses. A previous research study by Ashraf et al. [21] also demonstrated the effectiveness of RSM. The Pressure-Velocity Coupling PISO algorithm was preferred as the solution method, and spatial discretization was performed using a second-order upwind scheme. Time integration was handled with a fully implicit scheme, and convergence was considered to be achieved when the normalized residual value reached 1×10^{-6}. A detailed description of the algorithm and turbulence model can be found in the user manual [22]. Additionally, when analyzing the shape and formation of the interface between two or more immiscible fluids, the volume of fluid (VOF) model, which can be applied to a fixed Eulerian solution framework, is commonly employed [25]. In this research, the VOF method was used to compute the water-air interface. The VOF method identifies whether cells are empty, partially filled, or filled with water. A fluid volume (F) represents the filling ratio. For F=1, the element is filled; for F=0, it is filled with air; and for 0<F<1, the network element is partially filled. The "Geo-Reconstruct" approach was applied in calculating the free water surface using the VOF [22]. According to this approach, the position of the air-water linear interface is initially determined relative to the center of gravity, based on data regarding the ratio and its derivatives for each partially filled cell. Subsequently, the fluid amounts transported across each surface are computed using the determined linear interface position along with tangential velocity information calculated at the element surfaces. Finally, considering the fluid amounts computed previously, the filling ratio of each cell is determined by applying the continuity equation. Figure 2 is an example of the fullness ratio of the water-air interface in a region.

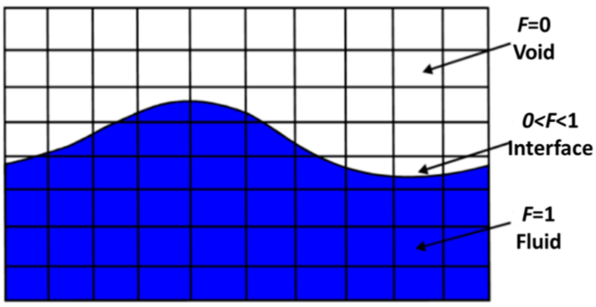

Figure 2. Fill rate of mesh elements with VOF model [26].

In the present study, in order to ensure mesh independence, three different mesh sizes were used to ensure the precision and reliability of the simulations. For this purpose, analyses were performed as coarse mesh (0.4 million), medium mesh (0.85 million), and fine mesh (1.9 million). Verification of mesh independence was obtained by comparing the simulated and experimental data of Anjum et al. [24]. The observed differences were approximately 9% for coarse and medium mesh cases and approximately 2% for medium and fine mesh cases. As a result, a 0.85 million mesh structure was considered for the present study. In addition, the “Average Skewness and Average Orthogonal Quality” values, which are important parameters for mesh precision, were examined. While the Average Skewness value was 0.22~0.23 for Case-1 and Case-2, respectively, the Average Orthogonal Quality values were obtained as 0.76~0.77. Figure 3 depicts the layout of the 3D area.

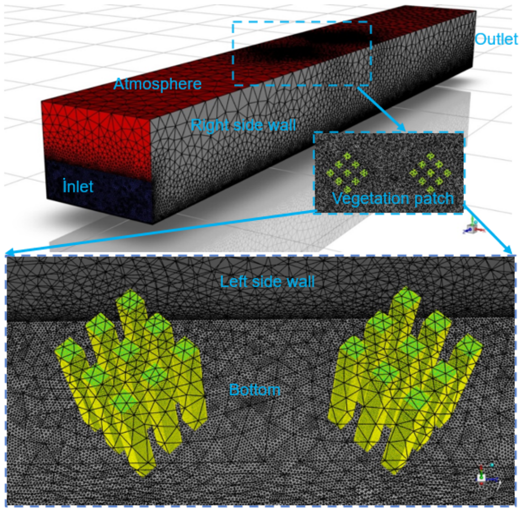

Figure 3. Boundary conditions and mesh structure.

2.3. Numerical model validation

The numerical model validation is given in Figure 4a. For this validation, the RSM model was tried to be validated using the experimental data of Anjum et al. [23]. The velocity values for the experiments and simulation were measured vertically at point P on the downstream side of the vegetation patch, as shown in Figure 4b. In addition, the vertical depth of the flow (h) is shown on the y-axis, while the velocity magnitudes in the flow direction (u) are shown on the x-axis. The results of the RSM model for the flow direction velocity are in a consistent trend with the experimental results in all numerical experiments. However, there is a slight difference between the experimental and numerical results near the top and bottom of the vegetation. This situation is also stated by Anjum et al. [24], which is attributed to the intense turbulence at the water-vegetation patch interface and the inevitable measurement error of the sensor of the velocity measuring device.

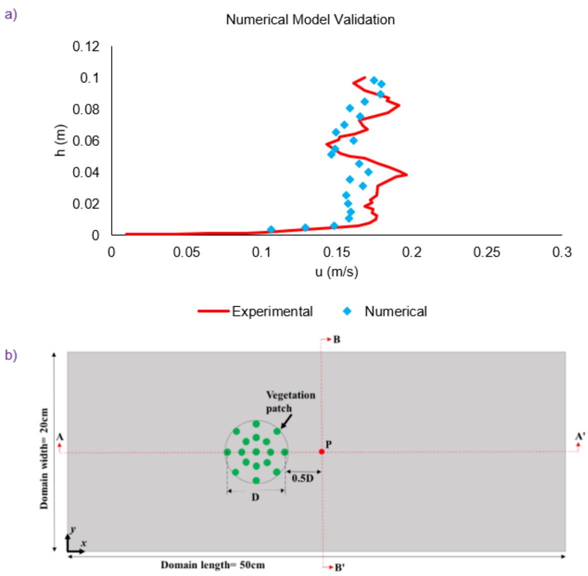

Figure 4. a) Validation of numerical model data with that of experimental data b) Flow field and experimental and numerical measurement point of Anjum et al. [24] study.

3. Results and Discussion

To measure the vertical velocity profile, a vertical line (at position P1) was drawn along the water depth at the center of the CFD channel, just below the vegetation patch (0.5D). In Figure 5a, the vertical velocity distribution profile of the vegetation patch for Case-1 and Case-2 was measured at the same point. The velocity profiles were affected behind the vegetation patch due to the drag provided by the square vegetation and therefore showed some fluctuations, which were observed to change according to the configuration, i.e., the number of patches. Accordingly, velocity values close to zero were obtained at the channel bottom for Case-1 and Case-2 due to the bed resistance. In addition, the velocity in Case-1 showed a sharp increase from 0 to 0.158 $m.s^{-1}$ relative to the vegetation patch. After this point, the increase in velocity was more gradual and decreased the flow velocity by 57% relative to the flow velocity at the inlet. A similar situation was observed for Case-2, where the velocity distribution about the vegetation patch showed a sharp increase from 0 to 0.176 $m.s^{-1}$ as the height increased. After this point, the increase in velocity was more gradual and decreased the flow velocity by 52% compared to the flow velocity at the inlet. The vertical velocity distribution for both cases within the P2 point of the CFD medium is obtained in Figure 5b. The velocity measured at the P2 point in Case-1 showed a sharp increase from 0 to 0.4 $m.s^{-1}$ as the height increased and reached values higher than the flow velocity at the channel entrance. Afterwards, it continued to decrease gradually towards the top of the vegetation. At the P2 point of Case-2, there was a sharp velocity increase from 0 to 0.09 $m.s^{-1}$ as the flow depth increased. Although it showed a partial decreasing trend afterwards, it increased up to 0.15 $m.s^{-1}$. Afterwards, the flow velocity showed a decreasing trend and continued with values close to a constant velocity when the flow depth was approximately 0.13 m. This situation shows that an effective velocity distribution is provided as a result of the two-row arrangement of the vegetation patches. The flow from the first vegetation patch encounters the second vegetation patch, which creates a sharp flow separation in the flow steering effect of the vegetation patch and the downstream interface, leading to strong eddies and increased energy dissipation. This is directly caused by the sudden momentum change caused by the square vegetation patches [24].

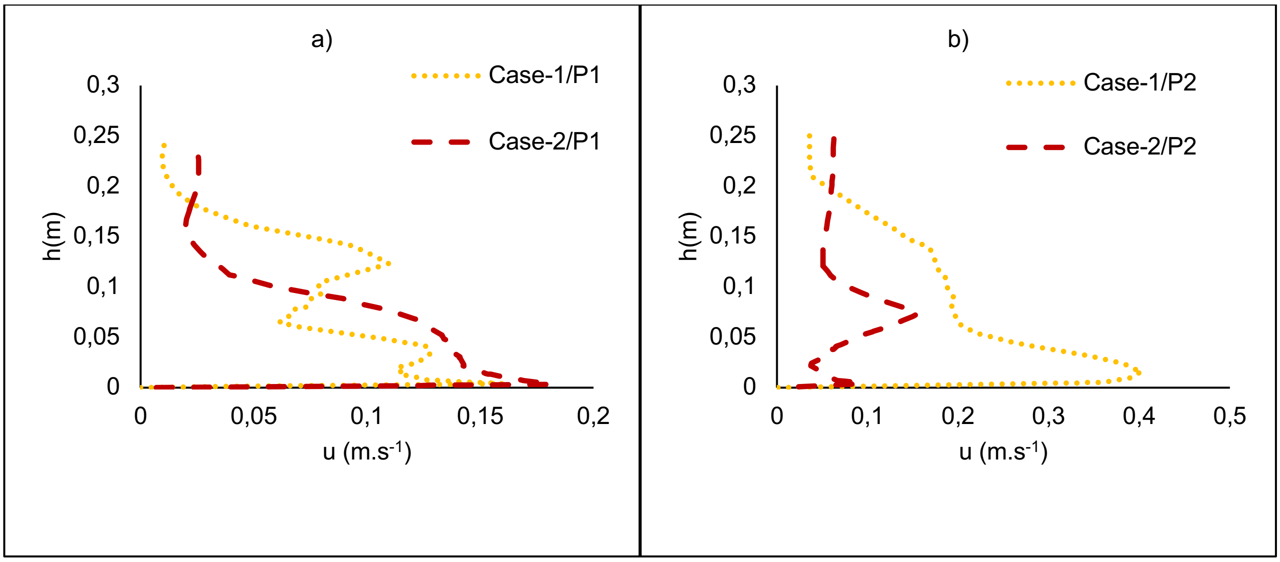

Figure 5. Depth-averaged vertical velocity distribution at points P1 and P2 for Case-1 and Case-2.

In Figure 6, Turbulent Kinetic Energy (TKE) values were obtained at y=0.03 m above the channel bottom. Higher TKE values mean that more energy is absorbed. These values can be said for Case-1 that the V-shaped parts downstream of the vegetation patch increase the TKE values, and that 0.05 $m^2.s^{-2}$ values are obtained more in this region. It can be said that more energy is dissipated at the vegetation patch outlet. In addition, TKE values almost close to 0 were obtained in the channel center axis immediately downstream of the patch, and then the TKE values partially increased towards the channel side walls in an inverted V shape.

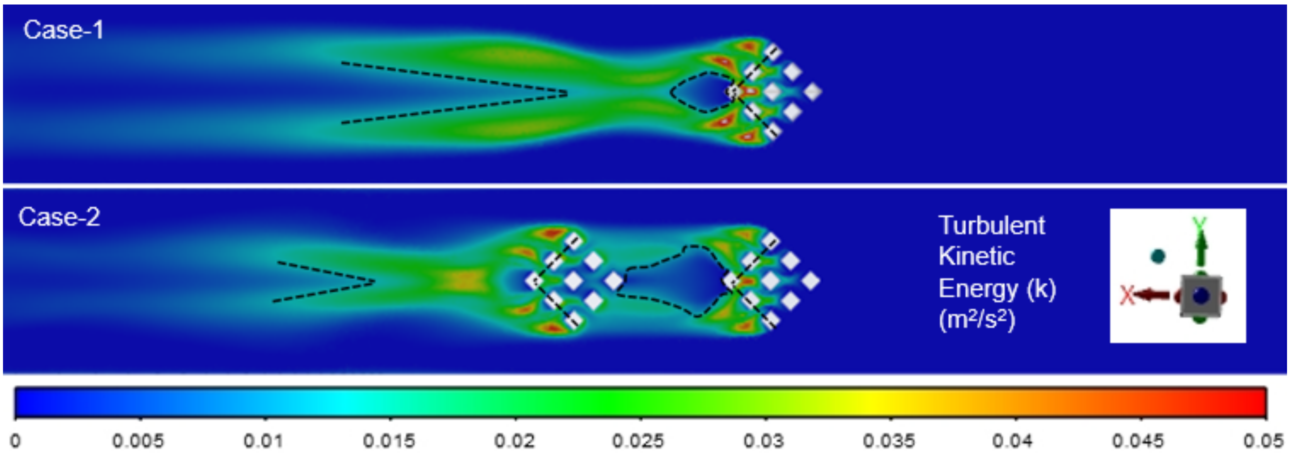

Figure 6. TKE values for Case-1 and Case-2 at y=0.03.

For Case-2, higher TKE values were observed in the downstream patch compared to the patch close to the upstream. TKE values close to 0 were observed more in the region between the two patches. In addition, the TKE region in the inverted V shape became smaller after the downstream patch. In terms of the effect in the downstream region, the turbulence region in Case-2 became narrower compared to Case-1, and TKE values greater than 0 were observed in the channel center. This also tells us that more energy is dissipated. The values obtained in Table 2 show this.

Table 2. Energy dissipation conditions for Case-1 and Case-2.

Case no	h_1	V_1	h_2	V_2	E_1	E_2	$\Delta E=(E_1-E_2)/E_1$
Case-1	0.1233	0.362	0.08	0.44	0.129979	0.089867	0.30860
Case-2	0.1233	0.362	0.04	0.81	0.129979	0.073440	0.43499

The energy (E) at any section of the open channel is calculated with the specific energy equation below.

$$E=h+\frac{V^2}{2g} \tag{1}$$

Here is the energy difference between the two points:

$$\frac{E_1 - E_2}{E_1} = \frac{\Delta E}{E_1} = \left[\frac{(h_1 + \frac{V_1^2}{2g}) - (h_2 + \frac{V_2^2}{2g})}{(h_1 + \frac{V_1^2}{2g})}\right] \tag{2}$$

and percent energy loss,

$$\% \frac{\Delta E}{E_1} = \left(\frac{E_1 - E_2}{E_1}\right) x100 \tag{3}$$

$\Delta E(\%)$: the percent energy dissipation, E: the specific energy of the flow (as well as its total energy if the channel bed is assumed horizontal), n is the cross-section number of the channel, h: the flow depth, V: the average velocity of the flow, g: the gravitational acceleration. The indices 1 and 2 in the equations represent the upstream and downstream of the open channel, respectively.

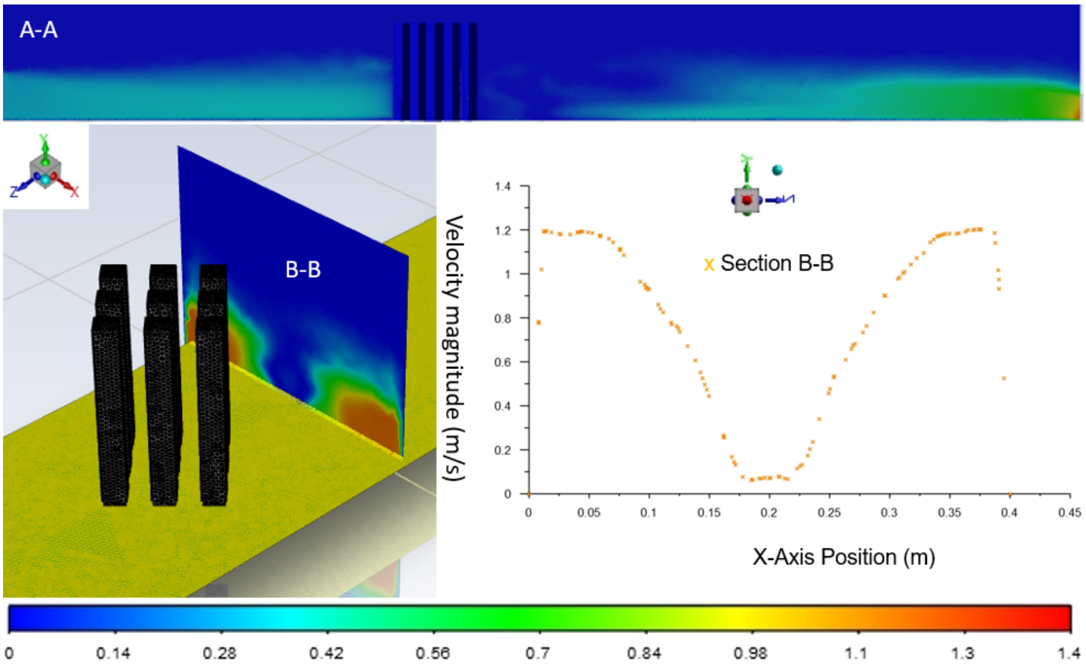

a)

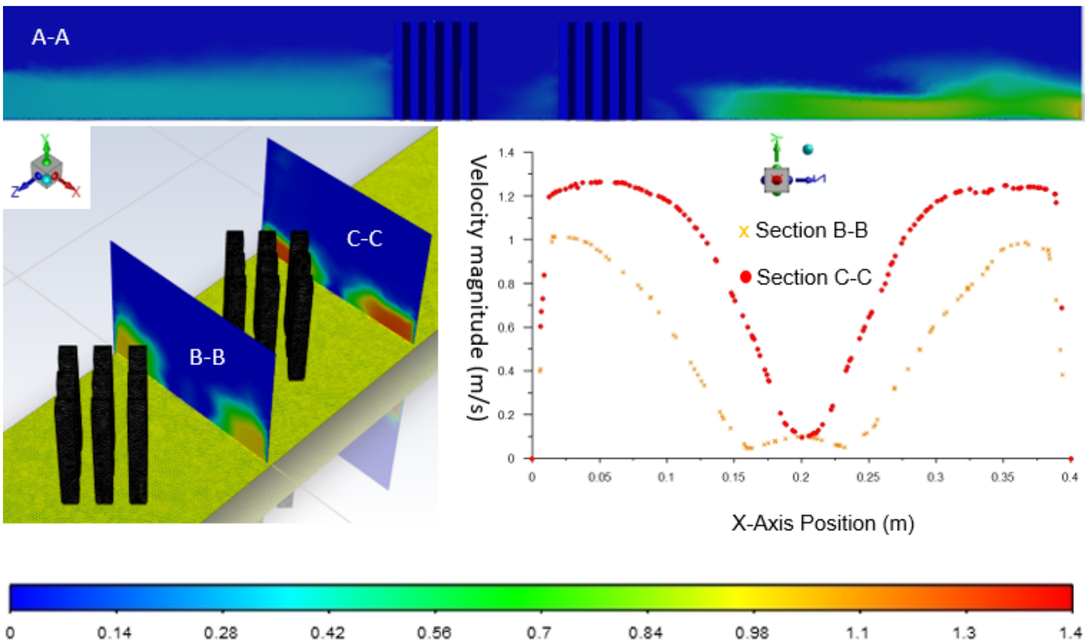

b)

Figure 7. Velocity contours in sections A-A, B-B and C-C and a) Section velocity distribution passing through 0.5D for Case-1 b) Section velocity distribution passing through 0.5D at both patch downstream for Case-2.

In Figure 7, the velocity contours taken in sections A-A, B-B and C-C and the velocities downstream of the vegetation patch are observed. Figure 7a describes Case-1. Section A-A passes through X=0.2 m, that is, the channel mid-axis. While the velocities remained at very low values, especially in the region with vegetation patches and upstream, the flow velocity showed an increasing trend towards the downstream side. In section B-B, while the flow velocity was around 0.1 $m.s^{-1}$ in the channel mid-axis, the vegetation pieces dividing the flow into two and directing it towards the downstream side caused velocity increases of up to 1.2 $m.s^{-1}$ in the channel edge region. Figure 7b expresses the observations obtained for Case-2. In section A-A, very low flow velocities were observed in the vegetation patch and the upstream region. For section B-B, while the velocity was at a very low level in the channel mid-axis, it increased up to 1 $m.s^{-1}$ towards the channel side walls. In the C-C section, the flow velocities increased up to 1.2 $m.s^{-1}$ towards the channel side surfaces. This situation can be said to cause an increase in speed as the flow passing through the first vegetation patch row tries to pass through a narrower area in the second vegetation patch.

4. Conclusions

The effect of the quadratic elements of rigid vegetation patches on the flow dynamics by providing a diamond arrangement is the focus of this study. A CFD approach was applied to visualize the detailed flow structures, velocity distribution, depth-averaged velocity distribution, and TKE around the vegetation patches in single-row and double-row arrangements. Accordingly, it was observed that the patches with double-row arrangements resulted in a more effective velocity distribution. The depth-averaged vertical velocity distribution at points P1 and P2 showed that lower values were obtained at the downstream for Case-2. The vegetation patch in Case-1 showed a sharp increase from 0 to 0.158 $m.s^{-1}$. After this point, the increase in velocity was more gradual and decreased the flow velocity by 57% compared to the flow velocity at the inlet. Similarly, the velocity distribution to the vegetation patch for Case-2 showed a sharp increase from 0 to 0.176 $m.s^{-1}$ as the height increased. After this point, the increase in velocity was more gradual and decreased the flow velocity by 52% compared to the flow velocity at the inlet. In addition, in terms of the effect in the downstream region, the turbulence region in Case-2 narrowed even more compared to Case-1, and TKE values greater than 0 were observed in the channel center. This also tells us that more energy was dissipated. While the energy dissipation percentage was 30% for Case-1, approximately 43% dissipation was achieved in Case-2. In the velocity graph obtained for the A-A section taken along the channel center axis and for the cross sections B-B and C-C, velocity increases were observed in the downstream. It can be said that this situation, especially for Case-2 caused an increase in speed because the flow passing the first vegetation patch row tried to pass in a narrower area in the second vegetation patch. Thus, it caused the flow depth to decrease. The obtained results are important for determining the effect of rigid vegetation patches on the flow dynamics. In addition, the support of CFD sampling with visuals and big data opportunities for feasibility reporting before field applications is at the forefront.

References

[1] **Fonseca, M. S.,** & Kenworthy, W. J. (1987). Effects of current on photosynthesis and distribution of seagrasses. *Aquatic botany*, *27*(1), 59-78.

[2] **Nepf, H. M.** (2012). Flow and transport in regions with aquatic vegetation. *Annual review of fluid mechanics*, *44*(1), 123-142.

[3] **Altun, Ö.** (2007). Bitki örtüsü içeren bileşik kesitli kanallarda kapasite tayini yaklaşımlarının model deneylerine göre irdelenmesi (Doctoral dissertation, Yüksek Lisans Tezi, Gazi Üniversitesi Fen Bilimleri Enstitüsü, Ankara).

[4] **Bai, Y.,** Han, L., Zhao, Y., Huang, L., Wang, Q., & Sun, G. (2024). Numerical simulation of velocity distribution and pollution transport in a two-stage channel with vegetation on a floodplain. *Journal of Hydrology*, *630*, 130788.

[5] **Asif, M.,** Ghani, U., Pasha, G. A., Ullah, M. K., & Ali, S. (2024). 3D numerical investigation of flow behavior in an open channel with uniform and layered vegetation patches under varying submergence conditions. *Ain Shams Engineering Journal*, *15*(1), 102288.

[6] **Pasha, G. A.,** & Tanaka, N. (2017). Undular hydraulic jump formation and energy loss in a flow through emergent vegetation of varying thickness and density. *Ocean Engineering*, *141*, 308-325.

[7] **Nikora, N.,** Nikora, V., & O'Donoghue, T. (2013). Velocity profiles in vegetated open-channel flows: combined effects of multiple mechanisms. *Journal of Hydraulic Engineering*, *139*(10), 1021-1032.

[8] **Belcher, S. E.,** Jerram, N., & Hunt, J. C. R. (2003). Adjustment of a turbulent boundary layer to a canopy of roughness elements. *Journal of Fluid Mechanics*, *488*, 369-398.

[9] **Luhar, M.,** Rominger, J., & Nepf, H. (2008). Interaction between flow, transport and vegetation spatial structure. *Environmental Fluid Mechanics*, *8*, 423-439.

[10] **Rominger, J. T.,** & Nepf, H. M. (2011). Flow adjustment and interior flow associated with a rectangular porous obstruction. *Journal of Fluid Mechanics*, *680*, 636-659.

[11] **Sukhodolov, A. N.,** & Sukhodolova, T. A. (2012). Vegetated mixing layer around a finite-size patch of submerged plants: Part 2. Turbulence statistics and structures. *Water Resources Research*, *48*(12).

[12] **Aydogdu, M.** (2023). Analysis of the effect of rigid vegetation patches on the hydraulics of an open channel flow with Realizable k-ε and Reynolds stress turbulence models. *Flow Measurement and Instrumentation*, *94*, 102477.

[13] **Wang, C.,** Zheng, S. S., Wang, P. F., & Hou, J. (2015). Interactions between vegetation, water flow and sediment transport: A review. *Journal of Hydrodynamics*, *27*(1), 24-37.

[14] **Sabokrouhiyeh, N.,** Bottacin-Busolin, A., Nepf, H., & Marion, A. (2016). Effects of vegetation density and wetland aspect ratio variation on hydraulic efficiency of wetlands. *Hydrodynamic and Mass Transport at Freshwater Aquatic Interfaces: 34th International School of Hydraulics*, 101-113.

[15] **Yılmazer, D.,** Ayna, G., Ozan, A. Y., & Cihan, K. (2022). Tam batmış bitki tarlasının açık kanal akım hızlarına etkisinin flow-3d ile modellenmesi. *Balıkesir Üniversitesi Fen Bilimleri Enstitüsü Dergisi*, *24*(2), 757-769.

[16] **Yılmazer, D.,** Ozan, A. Y., & Cihan, K. (2018). Flow characteristics in the wake region of a finite-length vegetation patch in a partly vegetated channel. *Water*, *10*(4), 459.

[17] **Cui, J.,** & Neary, V. S. (2008). LES study of turbulent flows with submerged vegetation. *Journal of Hydraulic Research*, *46*(3), 307-316.

[18] **Anjum, N.,** & Tanaka, N. (2019). Numerical investigation of velocity distribution of turbulent flow through vertically double-layered vegetation. *Water Science and Engineering*, *12*(4), 319-329.

[19] **Ghani, U.,** Anjum, N., Pasha, G. A., & Ahmad, M. (2019). Numerical investigation of the flow characteristics through discontinuous and layered vegetation patches of finite width in an open channel. *Environmental Fluid Mechanics*, *19*(6), 1469-1495.

[20] **Dissanayaka, K. D.,** & Tanaka, N. (2023). Comparison of the flow around circular and rectangular emergent cylinders with subcritical and supercritical conditions. *Fluids*, *8*(4), 124.

[21] **Ashraf, J.,** Anjum, N., Rahman, M. A., Ghani, U., & Ahmed, Z. (2024). Investigating the flow structure around floating vegetation islands in an open channel. *Innovative Infrastructure Solutions*, *9*(5), 159.

[22] **Ansys,** I. (2019). ANSYS Fluent User's Guide, Version 2019 R3. *ANSYS Inc., Canonsburgh, PA, USA*.

[23] **Anjum, N.,** Pasha, G. A., Ashraf, J., Ghani, U., Abbas, F. M., & Rahman, M. A. (2025). How emergent vegetation patch shapes affect flow structure in open channel environments. *Ecohydrology*, *18*(2), e2740.

[24] **Li, D.,** Liu, M., & Huai, W. (2022). Modeling transverse momentum exchange in partially vegetated flow. *Physics of Fluids*, *34*(2).

[25] **Hirt, C. W.,** & Nichols, B. D. (1981). Volume of fluid (VOF) method for the dynamics of free boundaries. *Journal of computational physics*, *39*(1), 201-225.

[26] **Jiang, H.,** Zhao, B., Dapeng, Z., & Zhu, K. (2023). Numerical simulation of two-dimensional dam failure and free-side deformation flow studies. *Water, 15(8),* 1515.

[27] **Craft, T. J.**, Launder, B. E., & Suga, K. (1996). Development and application of a cubic eddy-viscosity model of turbulence. *International Journal of Heat and Fluid Flow*, *17*(2), 108-115.

[28] **Chen, S. C.,** Kuo, Y. M., & Li, Y. H. (2011). Flow characteristics within different configurations of submerged flexible vegetation. *Journal of Hydrology*, *398*(1-2), 124-134.